

**Multiplexed Holographic Data Storage in  
Bacteriorhodopsin**

First Year Performance Report Submitted

to the

NASA Ames Research Center

MS 241-1

Moffett Field, CA 94035

by the

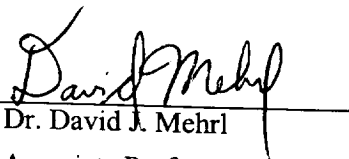
Optical Systems Laboratory

Department of Electrical Engineering

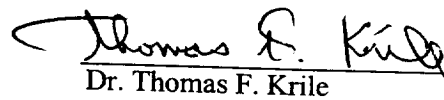
Texas Tech University

Lubbock, TX 79409-3102

July, 1997

  
Dr. David J. Mehrl

Associate Professor  
Principal Investigator

  
Dr. Thomas F. Krile

Professor  
Co-Principal Investigator

INTERIM  
IN 30-12  
OCIT  
055207

NA 62-1097  
#1

## MULTIPLEXED HOLOGRAPHIC DATA STORAGE IN BACTERIORHODOPSIN

**Abstract:** High density optical data storage, driven by the information revolution, remains at the forefront of current research areas. Much of the current research has focused on photorefractive materials (SBN and LiNbO<sub>3</sub>) and polymers, despite various problems with expense, durability, response time and retention periods. Photon echo techniques, though promising, are questionable due to the need for cryogenic conditions. Bacteriorhodopsin (BR) films are an attractive alternative recording medium. Great strides have been made in refining BR, and materials with storage lifetimes as long as 100 days have recently become available. The ability to deposit this robust polycrystalline material as high quality optical films suggests the use of BR as a recording medium for commercial optical disks. Our own recent research has demonstrated the suitability of BR films for real time spatial filtering and holography. We propose to fully investigate the feasibility of performing holographic mass data storage in BR. Important aspects of the problem to be investigated include various data multiplexing techniques (e.g. angle- amplitude- and phase- encoded multiplexing, and in particular shift-multiplexing), multilayer recording techniques, SLM selection and data readout using crossed polarizers for noise rejection. Systems evaluations of storage parameters, including access times, memory refresh constraints, erasure, signal-to-noise ratios and bit error rates, will be included in our investigations.

## INTRODUCTION

Bacteriorhopsin(BR) provides an attractive medium for optical signal/image processing and optical memory applications. Attractive features of BR include its relatively low cost, ability to deposit it in high quality optical films on planar or convex/concave surfaces, and its low sensitivity to environmental factors such as temperature/humidity fluctuations.

Our work with BR started several years ago, when M.S. student Jin Choi investigated holographic multiplexing techniques, using angle- and phase-encoding to multiplex multiple 2-D data patterns within a single BR film.

The current NASA grant began in September of 1996, and the research has been carried out largely by Post-doctoral research assistant Arkady Bablumian. The objective of this research is to investigate BR for use in optical (holographic) memory applications. A major part of this investigation is to explore various holographic multiplexing techniques (angle, amplitude- shift- and phase-encoded- multiplexing), and model and measure various performance parameters. Emphasis has been placed particularly on shift-multiplexing techniques, due to their mechanical simplicity and effectiveness (which makes them particularly viable for commercial application).

Our first year research results have resulted in several novel approaches, applicable not only to BR-based memories, but to other optical memories as well. Novel approaches include use of highly divergent spherical reference beams (quasi-point sources implemented using optical fibers), coupled with the use of differing wavelengths for hologram recording and readout (to improve diffraction efficiency and remedy the problem of "destructive readout"). A great deal of modeling and experimental work (diffraction efficiency, cross-talk, spatial resolution, etc.) has also been carried out on these approaches.

Much of our first year research focused on characterizing the response of BR films, devising robust methods for implementing shift multiplexing, and modeling and experimental measurement of basic multiplexed holographic optical memory architectures. To facilitate these investigations, experiments employed real-time (i.e. read and write is performed simultaneously - and often continuously as well) holographic techniques using short-lived BR films. Although the real-time techniques employed in the first year's research have little or no bearing in optical memory systems, they facilitated alignment, testing and measurement of BR parameters, and enabled us to perfect the differing wavelength and point source reference beam approaches that will likely be employed in the final BR-optical memory demonstration system.

In the second year, we will construct, demonstrate, model, and perform detailed measurements on a BR-based shift multiplexed holographic memory using longer-lived BR films. This will enable us to perform a myriad of systems level measurements such as access times, memory refresh constraints, erasure and exposure scheduling issues, signal-to-noise ratios, cross-talk and bit error rates. In addition, we expect to perform some investigation into the use of multi-layer BR media, as a means of improving the readout selectivity of multiplexed holograms (i.e. reducing crosstalk).

## **SUMMARY OF PROGRESS DURING YEAR ONE**

- Developed a novel shift multiplexing approach that utilizes an addressable array of point sources (implemented with optical fibers). This technique has also been coupled with the use of differing read and write wavelengths to remedy problems associated with destructive readout. We have also modeled this approach, and shown experimental results to agree with our theory.
- Developed the necessary infrastructure necessary to carry out research planned for year two (SLM input, frame grabber output hardware, automated shutter systems for exposure scheduling, automated precision positioning system etc.).
- Obtained and developed computer-based control software for the 2-axis precision positioning system that will be used for accessing the shift multiplexing demonstration system that will be developed in year two of the research program.
- A visit was made to NASA Ames, February 1997, by D.J. Mehrl, J.F. Walkup and J. Choi. A progress report was presented by D.J. Mehrl.
- Two conference papers have been presented (see bibliography), and an article has been submitted to Applied Optics (currently in review). Copies of these papers are included in the attached Appendix.

## **Research Plan for Year Two**

- Acquire long-lived BR films from Bend Research, and construct a demonstration setup of a shift-multiplexed BR-based optical memory. Construct an experimental testbed. Perform numerous system level measurements.
- Continue modeling of the BR shift-multiplexed memory architecture, and compare theoretical predictions with experimental results.
- If feasible, investigate use of multi-layer BR media in order to reduce crosstalk.

## **PUBLICATIONS - YEAR ONE**

### **Conference Papers:**

A.S. Bablumian, T.F. Krile, D.J. Mehrl, and J.F. Walkup, "Recording Shift-Selective M-Type Volume Holograms in Bacteriorhodopsin", SPIE Proc., Vol. 3159, SPIE Annual Technical Symposium, San Diego, CA, July 1997.

A.S. Bablumian, T.F. Krile, D.J. Mehrl, and J.F. Walkup, "Grating-Type Spatial Light Modulator in Bacteriorhodopsin Film", presented at the 1997 Gordon Research Conference on Optical Signal Processing and Holography, Meriden, NH, June 29-July 4, 1997.

### **Journal Papers:**

A.S. Bablumian, T.F. Krile, D.J. Mehrl, and J.F. Walkup, "M-type Thick Holograms in Bacteriorhodopsin Films with a High Divergence Reference Beam", Applied Optics, (in review).

## **PERSONNEL**

### **Faculty:**

Dr. David J. Mehrl, Principal Investigator  
Dr. Thomas F. Krile, Co-Principal Investigator  
Dr. John F. Walkup, Project Director

### **Students:**

Nabeen Surestha, Lab Assistant

### **Research Associate(Post-Doctoral):**

Arkady S. Bablumian

## **APPENDIX**

# **M-type thick holograms in Bacteriorhodopsin films with a high divergence reference beam**

**Arkady S. Bablumian, Thomas F. Krile, David J. Mehrl, and John F. Walkup**

**Department of Electrical Engineering**

**Texas Tech University**

**Lubbock, TX 79409**

## **Abstract**

The capability of using differing read and write wavelengths for reconstructing volume holograms recorded in a shift multiplexing geometry is analyzed and realized for M-type volume holograms recorded on Bacteriorhodopsin films. The intensity distribution in the reconstructed wave as a function of the parameters of the recording and readout beams is calculated. Optimal recording and retrieving geometry as well as a precise method for tuning the readout setup, are suggested.

**Keywords:** Bacteriorhodopsin, volume holograms, shift selectivity, differing read-write wavelengths, holographic data storage.

## **1. Introduction**

High capacity storage of optical information can be achieved by holographic recording throughout the volume of a thick medium [1]. The strong sensitivity of thick holograms to the parameters of the reconstruction beam allows one to multiplex many holograms in the same volume and then read them out selectively. The simplest way to retrieve any desired hologram is to use a readout beam identical, in all respects, to the reference beam used for

recording. At the same time, for nondestructive retrieval of stored holograms, it is necessary to either fix them or reconstruct them at wavelengths to which the material is insensitive. (The latter is of particular interest in the general area of real-time optical data processing). In general, changing the readout wavelength will not only change the output's orientation (in accordance with the Bragg condition), but the shape of the wavefront as well. This leads to both a loss of information in the object beam, and to difficulties associated with synthesis of a readout beam with a complicated wavefront shape. The simplest case of reconstructing a volume hologram formed by two plane waves was considered by Kulich [2]. Unfortunately, from the practical point of view this approach cannot be applied for analyzing several interesting hologram multiplexing geometries in situations where recording beams are highly divergent spherical waves with arbitrary orientations. In this paper we consider the results of both theoretical and experimental investigations of the differing read-write wavelengths reconstruction of optical information stored in a thick hologram with a recording geometry that is highly sensitive to a shift of the readout beam [1]. For an arbitrary wavelength, we calculate the optimal parameters for both the readout spherical beam and the appropriate intensity distribution and resolution in the reconstructed beam. These parameters are then compared with values derived experimentally.

It is necessary to notice that the readout beam has to be calculated and oriented with respect to the hologram with high accuracy, according to the shift selectivity of a chosen setup [2]. Since the orientation has three degrees of freedom, and recording beams have to be measured with the above-mentioned accuracy, it becomes clear that the results cannot be easily applied without some practical method of finding the optimal location of the readout beam. So, our next step was to develop a method for tuning the readout setup. Finally,



experimental verification of the theory is demonstrated using M-type holograms in Bacteriorhodopsine (BR) films.

## 2. Theory

Let the hologram be recorded by reference ( $u_1$ ) and object ( $u_2$ ) waves as shown in Fig.1. In both recording arms the laser beams are expanded and then point-focused. This allows both the formation of a spherical reference beam and insertion of the information into the object arm, using a transparency with transmittance  $t$ . The scaled Fourier-transform of  $t$  is produced at the plane of the beam focus  $[(x_2, y_2)$  in Fig. 1]. Here we let  $(x_1, y_1)$  designate the coordinates of the spherical reference source and  $(x_2, y_2)$  designate the coordinates of the zeroth-order component of the Fourier-spectrum of transparency  $t$ .

The hologram of transparency  $t$  can itself be regarded as the superposition of an array of elemental holograms, each being formed by a pair of spherical beams, whose sources are located at the point  $(x_1, y_1)$ , and one of the points of the Fourier-plane  $(x_2 + \Delta x, y_2 + \Delta y)$  Fig. 1]. The hologram of the zeroth-order component of the Fourier-spectrum  $T$  [ $H(\Delta x, \Delta y) = H(0, 0)$ ], will determine the background in the reconstructed image  $I$ , where the holograms of higher-order components [ $H(\Delta x, \Delta y)$ ] will determine its resolution. It is evident, that each of the elemental holograms can be reconstructed by the beam whose parameters coincide with those of one of the recording beams. The existence of reconstructed beams whose wavelengths differ from the recording wavelength becomes clear from the following consideration. Each elemental hologram is recorded by point-source beams, therefore any of its small parts is described by the constant grating vector  $K$ . This means that for an arbitrary wavelength  $\lambda$  in every point  $(x, y)$  of the elemental hologram, two rays (incident and diffracted) oriented at the Bragg angle to the grating vector  $K$  are determined

unambiguously. Let us neglect the change in the grating vector  $K$  along the propagation path for each reconstructed ray in the hologram. In this case the lattice of rays combines to form only two beams which can be diffracted by this hologram and which, generally speaking, for an arbitrary wavelength  $\lambda$ , are not spherical. Let us consider the hologram reconstruction by a spherical wave with coordinate  $(x_3, y_3)$  and determine the Bragg mismatch angle,  $\delta$ , for its rays at every point of their crossing within the hologram. The assumption we have made above permits us to consider the diffraction of each pair of interacting rays independently and to calculate pointwise the diffraction efficiency of incident rays as a function of angle  $\delta$  in accordance with coupled-wave theory [4]. Thus we can calculate the intensity distribution in the reconstructed beam for every elemental hologram  $H(\Delta x, \Delta y)$ . Their sum corresponds to the Fourier-spectrum of the transparency  $t$  by which we can estimate the resolution in the reconstructed image.

As indicated in Fig.1, rays from the recording  $(x_1, y_1)$ ,  $(x_2, y_2)$  and reconstructing  $(x_3, y_3)$  sources to an arbitrary point  $(x, 0)$  on the recording medium make an angle  $\theta_i$  where

$$\theta_i = \arctan\left(\frac{x_i - x}{y_i}\right), \quad i = 1, 2, 3. \quad (2.1)$$

The Bragg angle at the same point is

$$\theta_{Bragg}(x) = \arcsin\left\{\frac{\lambda_1}{\lambda_2} \times \sin\left[\frac{\theta_1(x) - \theta_2(x)}{2}\right]\right\} + \frac{\theta_1(x) + \theta_2(x)}{2}, \quad (2.2)$$

which directly follows from the Bragg law written in common form [Ref.3] for readout ( $\lambda_2$ ) and recording ( $\lambda_1$ ) wavelengths. Consequently the Bragg mismatch angle  $\delta_{Bragg}$  is:

$$\delta_{Bragg}(x) = \theta_{Bragg}(x) - \theta_3(x). \quad (2.3)$$

We choose the coordinates of the point source reconstruction beam  $(x_3, y_3)$  in such a way that two of its rays, crossing the hologram at points  $(0,0)$  and  $(c,0)$ , make Bragg angles with the input plane (Eq. 2.2). We then determine the mismatch angle  $\delta_{\text{Bragg}}$  for the rest of the rays of the reconstructed beam and insert it into the relationship which expresses the angular sensitivity of a thick hologram

$$\eta = \left| \exp\left[-\frac{\alpha d}{c_s}\right] \times \exp[-i\xi] \times \frac{\exp[i(\xi^2 + v^2)^{0.5}] - \exp[-i(\xi^2 + v^2)^{0.5}]}{2\left(1 + \frac{\xi^2}{v^2}\right)^{0.5}} \right|^2, \quad (2.4)$$

where  $\xi = \frac{2\pi n}{\lambda_2} \delta_{\text{Bragg}} d \sin\left(\frac{\theta_1 - \theta_2}{2}\right)$ ;  $v = \frac{\chi d}{c_s}$ ;  $c_s = \cos\left(\frac{\theta_1 - \theta_2}{2}\right)$ .

where  $d$  is the thickness of the hologram and  $\chi$  is the coupling constant [Ref.4].

This expression describes, in the exit plane of the hologram, the profile of the intensity of the diffracted wave which attains its maximum at points  $x=0$  and  $x=c$ . Notice that we are interested in the relative diffraction efficiency of diffracted rays versus only  $\delta_{\text{Bragg}}$  for each of them, so we can simplify Eq. (2.4) to obtain

$$\frac{\eta}{\eta_0} = v^2 \sin^2 \left\{ \pi^{-1} \left[ v^2 + k \delta_{\text{Bragg}}^2(x) \right]^{0.5} \right\}. \quad (2.5)$$

Here we took into account the fact that the presence of loss has very little influence on the angular sensitivity [Ref.4] and used Eq. (2.4) written for lossless gratings with real  $\chi$ . The constant  $v$  was measured experimentally. Figure 2 represents the relative intensity distribution profile (equivalent to normalized diffraction efficiency) of diffracted beams in the exit plane of the hologram, calculated for the elemental hologram  $H(0,0)$  [corresponding to the zeroth-order component of the Fourier-spectrum,  $T$  of transparency  $t$ ] for

reconstructed beams with different values of the parameter 'c'. Values of  $\lambda_1=458\text{nm}$  and  $\lambda_2=633\text{nm}$  were used for this and subsequent plots. The X-axis is in the hologram recording plane and the different values of 'c' are obtained by changing the location of the reconstruction point source,  $(x_3, y_3)$ . Optimized readout parameters will correspond to the portion of the hologram where the curves of Fig. 2 have sufficient diffraction efficiency, say not less than  $1/e$ , and are as flat as possible. In our experiments, (Section 3), the hologram was about 3mm in extent, so  $c = 2\text{mm}$  would be optimal from Fig. 2.

Profiles of diffracted beams with optimized parameter 'c', calculated for several recording set-ups of  $H(0,0)$  holograms (with different orientations and average spatial frequencies of their recording beams) are shown in Fig. 3.

The diffraction of the beam, optimized for the reconstruction of the hologram  $H(0,0)$ , from the holograms  $H(\Delta x, \Delta y)$ , corresponding to the higher-order components of the Fourier-spectrum  $T$ , is shown in Fig.4. These plots represent the sum intensity distribution of beams diffracted by holograms  $H(\Delta x, \Delta y)$  and  $H(-\Delta x, -\Delta y)$ , where we use the fact that symmetric components of the Fourier-spectrum contain the same information. From Fig.4, we see that the relative diffraction efficiency decreases with increasing values of  $r$ , corresponding to holograms of higher components of the Fourier-spectrum,  $T$ . Thus the reconstruction system is acting like a low-pass filter, and one can use this curve to define an effective spatial cutoff frequency, at some particular value of relative diffraction efficiency ( $1/e$ ).

Let's consider now in more detail how the intensity profiles of beams, diffracted by elemental holograms (Figs. 2-4) can be utilized to determine the resolution and intensity distribution in the reconstructed image,  $t$ . Every point  $P$  of the recording transparency,  $t$  is formed by a cone of rays connecting it with points of the Fourier-spectrum (Fig.1), each of

which we took as an elementary point-source object beam of the elemental hologram. The part of the transparency,  $t$  in the vicinity of the point  $P$  will be reconstructed with resolution  $h$ , if all rays of a cone with base radius

$$r = \frac{0.61\lambda_1 D}{h} \quad (2.6)$$

have enough diffraction efficiency ( $\eta > \frac{\eta_0}{e}$ ), where  $r = (\Delta x^2 + \Delta y^2)^{0.5}$  is one of the coordinates of the Fourier-plane of the transparency  $t$ , and  $D$  is the distance between the plane of transparency  $t$  and its Fourier-transform plane,  $T$ . Taking into account the behavior of the plots in Fig. 4, the proper diffraction efficiency of only edge cone rays corresponding to the maximal-order components of the Fourier-spectrum will provide the required resolution. Then, it is easy to see that the intensity distribution of the reconstructed beam at the image plane corresponds to a profile of the beam diffracted by the  $H(0,0)$  hologram at its exit plane reduced in size by  $D_2 \cos \theta_{\text{aver}} / D_1$ , where  $D_1$  and  $D_2$  are the distances between the Fourier-plane of image  $i$  and, accordingly, the hologram and the plane of the image, and  $\theta_{\text{aver}}$  is the average incident angle of the reconstructing beam. Thus, the intensity and resolution in an arbitrary part of the reconstructed image  $T$  can be estimated by the profile of two beams diffracted by elemental holograms  $H(0,0)$  and  $H(\Delta x, \Delta y)$ , where  $\Delta x$  and  $\Delta y$  obey the condition of Eq.(2.6).

### 3. Experimental Results

To investigate the different wavelength regimes of recording and reconstructing volume holograms, we used a thick Bacteriorhodopsin(BR) film. This material exhibits excellent properties for real-time optical processing applications as well as for permanent high-density

data storage [Ref.3]. The hologram recording in BR-films was carried out in the M-type regime, where the readout red light performed, at the same time, the excitation function for the BR molecules, transferring them into the state (M-state) ready for recording by blue light. M-type holograms were used as an example of nondestructive restoration, which simultaneously allows us to change and compare in real-time the recording and readout parameters. The mutant-variant BR<sub>D96N</sub>-films with a thickness of 100μm were used. The hologram of a standard USAF test-pattern was recorded at  $\lambda=458\text{nm}$  and reconstructed at  $\lambda=633\text{nm}$ . The setup geometry for recording and reconstruction was chosen according to the theory above enabling us to compare experiments results with the results derived theoretically (see Figs. 2 - 4).

As was pointed out above, in the recording regime, with a high-sensitivity to shift, the process of finding the location of the readout beam with the given parameters becomes a practically difficult problem. This is particularly true for high values of the Klein parameter  $Q$ , which characterizes thick gratings. For optimally tuning the readout setup the following method was suggested and utilized. The thick recording medium was first replaced by a structure consisting of two separated thin films. The hologram recorded in such a structure, in contrast to a common thick hologram, can be reconstructed by any orientation of readout beams. This forms two images, propagated, in general, in different directions. Upon optimal orientation of the readout beam, these directions coincide and interferometric fringes of overlapped images coalesce into one fringe, by the maximal size of which one can judge the accuracy of the reconstruction source location. For such a structure, modeling the volume medium, a 1mm glass plate with photo resist layers on both surfaces was used. The readout beam was formed using a piece of optical fiber, so as to be able to manipulate the beam's

parameters in real-time. The setup allowed us to position the recording medium used in the same place and compensate for the influence of their different thicknesses on the setup parameters upon making the transition from the model medium to the BR-film.

Figure 5 presents the photos of the USAF image reconstructed from the BR-film with different values of the Q-factor. For comparison, next to each photo are shown (Fig 5) the plots of intensity profiles of beams diffracted from two elemental holograms  $H(0,0)$  and  $H(\Delta x, \Delta y)$  recorded in the corresponding geometry.

As one can see, the resolution (for instance  $30\mu\text{m}$ ) conforming to plots 2a, 2b, and 2c on Fig. 5 is provided all over the field of the reconstructed image for  $Q=100$  and  $300$ , and reduced in some parts for  $Q=750$ , which is supported upon analysis of the corresponding photos. The experimental sensitivity of the setup with  $Q=750$  to the shift of the readout beam was approximately  $20\mu\text{m}$ , deviating by 5%-6% from the theoretical prediction. The measured diffraction efficiency of the reconstructed images was approximately 4%-5%.

#### **4. Conclusions**

We have demonstrated a relatively simple method of calculating critical parameters for the process of reading & writing volume holograms using highly divergent beams of differing wavelengths. Experimental results were shown to agree with theoretical results. We considered the resolution and relative intensity distribution of the reconstructed image stored in the thick hologram by a high divergence reference beam which is arbitrarily oriented relative to the object beam. These parameters, as well as the optimal parameters of the readout beam, can be estimated by the intensity profiles of beams diffracted by two elemental holograms (recorded by a pair of spherical beams) whose simple calculation method has been presented above. A method for modeling a volume hologram using a

medium consisting of two separated thin layers was also suggested. This approach allows one to experimentally find the precise optimal position of the readout beam. Also, the method makes accessible the modeling and direct visualization of the process of diffraction by thick holograms with arbitrary recording parameters, which could be difficult or impossible due to the characteristics of commonly used volume recording media (e. g. low life times, low diffraction efficiency, destructive readout, etc.).

### **Acknowledgments**

We thank the Bend Research, Inc. for BR-films preparation. This work was supported by the NASA Ames Research Center, whose support is sincerely appreciated.

### **References**

1. G. Barbastathis, M. Levene, and D. Psaltis, "Shift multiplexing with spherical reference beam", *Applied Optics* **35**, 2403 (1996).
2. H.C. Kulich, "A new approach to read volume holograms at different wavelengths", *Opt. Com.* **64**, 407 (1987).
3. R.J. Collier, C. B. Burckhardt, and L. H. Lin in: *Optical Holography*, 128, (Acad. Press, New York. London, 1971)
4. H. Kogelnik, "Coupled wave theory for thick hologram gratings", *Bell. Syst. Tech. J.* **48**, 2909 (1969).



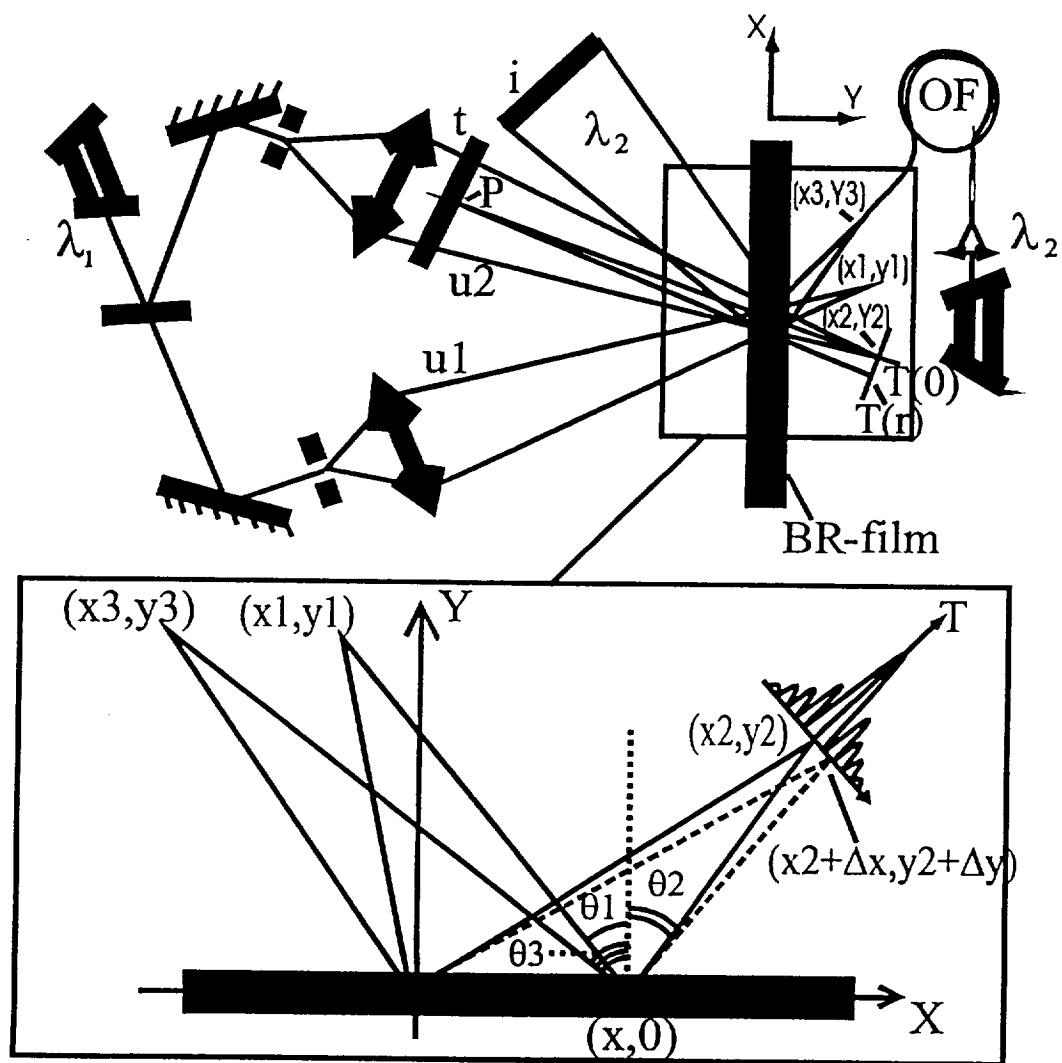
Fig. 1: Geometry of recording and readout rays. Here  $t$  and  $T$  denote the transparency and its scaled Fourier-transform respectively;  $i$  - reconstructed image; OF - optical fiber.

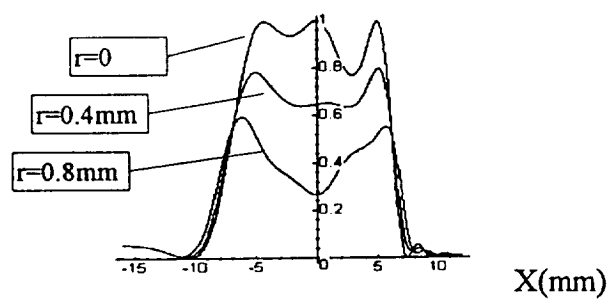
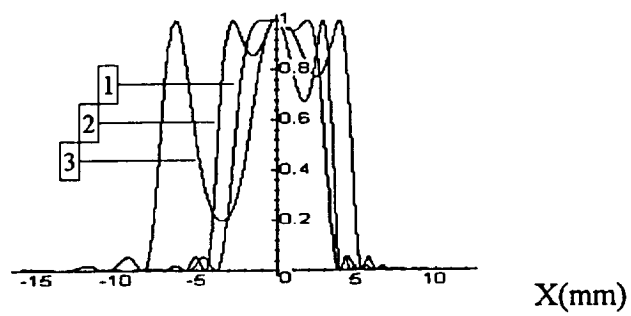
Fig. 2: Normalized diffraction efficiency of  $H(0,0)$  versus hologram plane position for various 'c' parameters.

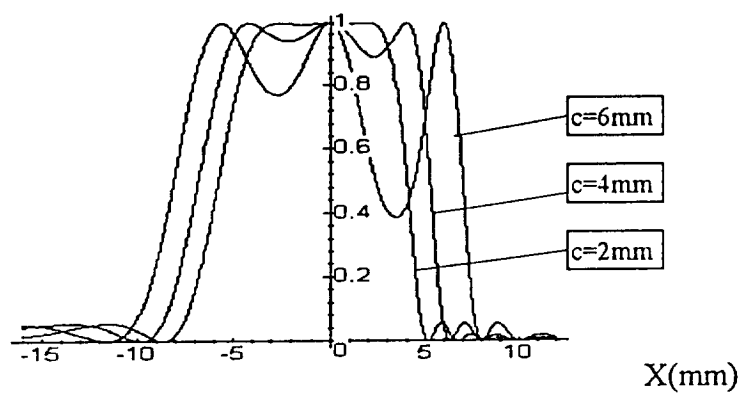
Fig. 3: Normalized diffraction efficiency for cases:  $(x_1, y_1) = (7, 10)$ ,  $(x_2, y_2) = (6.5, 10)$ ,  $(8, 10)$ ,  $(5, 10)$  - plots 1, 2, and 3, respectively.

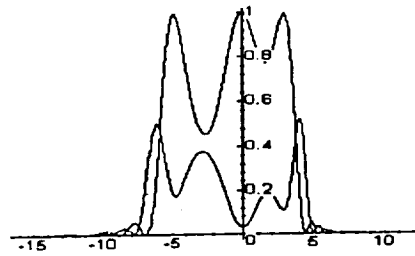
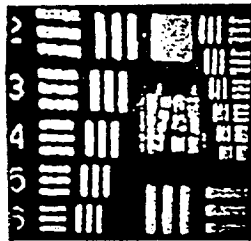
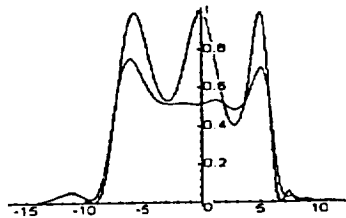
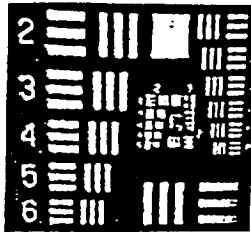
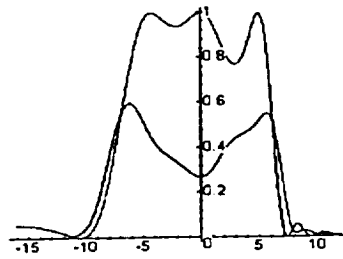
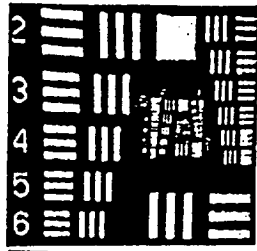
Fig. 4: Normalized diffraction efficiency of elemental holograms with various  $r$  versus hologram plane position.

Fig. 5: Photos of transparency  $t$  from hologram  $H$  and corresponding plots of reconstructed beams at two elemental holograms  $H(r=0)$  - plot 1 and  $H(r=1\text{mm})$  - plot 2 in exit plane of hologram  $H$  for  $Q=100$  (a),  $Q=300$  (b), and  $Q=750$  (c).









## Recording shift-selective volume holograms in Bacteriorhodopsin

Arkady S. Bablumian, Thomas F. Krile, David J. Mehrl, and John F. Walkup  
Department of Electrical Engineering  
Texas Tech University  
Lubbock, TX 79409

### Abstract

The application of volume M-type holograms for building multichannel geometries in pattern recognition systems is considered. The results of theoretical and experimental investigations of the hologram's parameters as a function of their recording parameters and their use as filters in correlation setups are presented. Multichannel correlation schemes where the processed signals have either different or the same wavelength are proposed. We have shown that all the correlation schemes proposed allow one to increase data throughput several times over single-channel BR-based correlators.

**Keywords:** Bacteriorhodopsin, volume hologram, hologram multiplexing, optical correlator

### 1. Introduction:

The bistable nature of the photocycle in Bacteriorhodopsin (BR) is commonly used in a wide area of optical storage and real-time processing application. BR applications for optical pattern recognition were suggested in [1-3]. In these papers experimental results of signal processing in correlation systems with a fixed input pattern [1], as well as the correlation of two video signals using BR dynamic properties [2, 3] were provided. In all these papers the process of M-type hologram recording was used [1], where the readout red light performed, at the same time, the excitation function for the BR molecules, transferring them into the state (M-state) ready for recording by blue light. All the BR-based correlation systems suggested in the above mentioned references were implemented using the geometry of the joint Fourier transform correlator (JFTC), since this geometry is similar to one used in recording and real time reconstruction of M-type holograms. At the same time the typical timing of photoreversible transitions between the excited (M) and the initial BR states (typically about 10 ms) limits data throughput of such correlators. The capacity of optical data processing can be increased in correlation systems which incorporate a multichannel geometry. Such systems should provide a way to record a hologram of several optical signals in real time simultaneously and also a way to reconstruct them selectively. Such requirements can be met by volume holograms working in the Bragg diffraction regime. To implement a multichannel geometry, a correlator with frequency plane (CFP) (Van-der-Lugt matched filter) seems more promising compared with the JFTC's used in the above mentioned references because of the following points:

1. In the JFTC the hologram that contains the correlation signal (as one of the diffraction orders) is recorded with the two signals being compared. Therefore the correlation signal formation time is determined by the time it takes to form the hologram in BR, which in turn is determined by the photoreversible transition time between the M and BR states.
2. JFTC requires different wavelengths during the recording and the reconstruction stages of the hologram that contains the correlation signal. Changing the readout wavelength not only will change the outputs' orientations (according to the Bragg condition [5]), but also the shape of the wavefront. In the JFTC, the wavefront shape of the reconstruction beam is significantly different from the wavefront shape of the recording beams (recording beams are the processed optical signals  $S_1$  and  $S_2$ , and the reconstruction beam as a rule has a planar wavefront). For large values of parameter  $Q$  (characterizing thick holograms) a decrease in diffraction efficiency and resolution is observed when the correlation signal is reconstructed. This fact limits thick hologram applications in the JFTC in principle.
3. On the other hand, in CFP the correlation signal represents the diffraction of one of the input signals  $S_2$ , by the hologram of the other signal  $S_1$ . Multiplexing several hologram-filters in the recording medium volume will allow one to increase proportionally the number of input signals being processed.

The purpose of our project was to increase data throughput in BR based pattern recognition systems (PRS). In this paper different options for building multichannel geometries for signal processing are considered. The following problems, for which solutions are necessary for creating such a PRS, have been investigated:

1. Real time recording of several holograms and their selective reconstruction in a BR film with a short life time (less than the exposure time of one hologram) (Sec. 2)
2. In Sec. 3 we consider the differing read-write reconstruction of optical information stored in a thick hologram with a recording geometry that is highly sensitive to a shift of the readout beam. For an arbitrary wavelength, we calculate both the optimal parameters for the readout beam and appropriate intensity distribution and resolution in the reconstructed beam. These parameters are then used for estimation of the loss of information associated with differing read-write reconstruction.
3. In Sec. 4, multichannel correlator schemes in which the compared signals can have different wavelengths as well as the same wavelength have been investigated. It has also been shown that, for correlators working with one wavelength (for all the compared signals and the correlation signal), one input spatial light modulator (SLM) can be used.

## 2. Hologram multiplexing in thick BR films with short lifetimes.

To solve the problem of simultaneous recording and selective reconstruction of holograms using BR films, we have used an encoding method analogous to shift multiplexing [4]. As in [4], we are using the strong selectivity of volume holograms to the parameters of the reference beam. However, unlike shift multiplexing that uses a shift of the recording medium, in our work each hologram of the input signals  $S_i = S_0 \exp[ik_i \cdot r]$  is recorded by shifting the reference beam (Fig. 1). Each reference beam  $R_i = R_0 \exp[ik_i \cdot r]$  is formed by a piece of optical fiber  $OF_i$ . The relative distance between the emitting edges of the  $OF_i$  was chosen sufficient to suppress the cross-talk noise during the reconstruction stage.

Coupling of laser beam with either fiber is done in node D which consists of an acousto optical deflector (AOD) and wide aperture microobjective  $O_i$ . Node D is adjusted so that at each moment one of the optical fibers  $OF_i$  is excited depending on the voltage applied to the deflector. The LC SLM, driven by a computer, was used to input the optical signals into the setup. The readout beam was formed also using a piece of optical fiber so as to manipulate the beam's parameters in real-time. The holograms have been recorded with wavelength  $\lambda_1 = 0.45 \mu$  and reconstructed with  $\lambda_2 = 0.63 \mu$ . Holograms were recorded in the M-type regime in which, as was mentioned above, the readout red beam performs, at the same time, the excitation function. The holograms have been recorded using the following method.  $N$  signals  $S_i$  are displayed on the SLM with frequency  $\nu$ . Reference beam switching is done at the same frequency. The SLM and AOD were synchronized so that each signal  $S_i$  from  $N$  signals  $S_n$  would correspond to a single reference beam  $R_i$  from  $N$  reference beams  $R_n (n=1 \dots N)$ . Thus each pair of beams  $(S_i, R_i)$ , representing the  $i$ -th hologram  $H_i$ , expose the recording medium with frequency  $\nu/N$  in the time interval  $1/\nu$ . In time  $N/\nu$ , the recording medium will be exposed to all holograms  $H_i$ . If this time is significantly less than the lifetime of the excited M-state of BR (determining the film's memory), then the recording conditions of the holograms are the same with respect to each other. To qualitatively evaluate the effect of recording  $N$  holograms on the diffraction efficiency of each individual hologram, we have to take into account the following:

Let's consider the average intensity  $I_0$  of each pair  $(S_i, R_i)$  to be the same, and pairs  $(S_i, R_i)$  themselves as uncorrelated (sequential recording) and assume high spatial frequency functions (interference pattern of the two coherent beams  $S_i$  and  $R_i$ ). In this case the total exposure  $E$  of the recording medium by all  $N-1$  holograms (except the  $i$ -th hologram) in each point of the recording medium is equal to:

$$E = T \left( \sum_{\substack{n=1 \\ n \neq i}}^N (S_i + R_i) \right)^2 = T \sum_{\substack{n=1 \\ n \neq i}}^N (S_i + R_i)^2 \approx T(N-1)I_0, \text{ where } T \text{ is exposure time.} \quad (2.1)$$

Thus the cumulative effect of  $N-1$  holograms on recording the  $i$ -th hologram can be considered as a uniform illumination (for large values of  $N$ ) of the recording region by a beam, the intensity of which exceeds  $N-1$  times the average intensity of recording pairs  $(R_i, S_i)$ . Figure 2a shows the diffraction efficiency of an M-type hologram as a function of intensity of a blue beam uniformly illuminating the recording region of the hologram. The plot is constructed for different values of the  $I_2/I_1$  ratio which are 1, 2, and 5, respectively. Figure 2b shows the similar plots of the DE versus units of the average blue intensity. It can be seen from Fig. 2b that by selecting a proper parameter ratio  $I_2/I_1$ , say curve 1, for small values of

N, say,  $N=4$  which corresponds to the  $(N-1)I_0=3I_0$  point, one obtains a factor of 5 decrease of diffraction efficiency, DE in hologram  $H_i$  compared to the single-exposure case, which will correspond to 0.5% - 0.8% for BR.

In our work, simultaneous hologram recording using the above described approach has been tested for the case  $N=2$ . Maximum diffraction efficiency of the holograms recorded in BR was 1-1.3% instead of the expected value of 2%, which was evaluated using Figures 2a, b.

Such a decrease (1.5 times) in diffraction efficiency can be explained by the instability of the voltage applied to the AOD, which leads to a phase drift of  $R_i$ , causing the diffraction efficiency to decrease.

### 3. The influence of differing read-write wavelength reconstruction on the parameters of the volume holograms

Let the hologram be recorded by reference ( $u_1$ ) and object ( $u_2$ ) waves as shown in Fig. 3. In both recording arms the laser beams are expanded and then point-focused. This allows both the formation of a spherical reference beam and insertion the information into the object arm, using a transparency with transmittance  $t$ . The Fourier-transform of  $t$  is produced at the plane of the beam focus  $(x_2, y_2)$  in Fig. 3]. Let  $(x_1, y_1)$  designate the coordinates of the spherical reference source and let  $(x_2, y_2)$  designate the coordinates of the zeroth-order component of the Fourier-spectrum of transparency  $t$ .

The hologram of transparency  $t$  can be regarded as the superposition of an array of elemental holograms, each being formed by a pair of spherical beams, whose sources are located at point  $(x_1, y_1)$ , and one of the points of the Fourier-plane  $(x_2 + \Delta x, y_2 + \Delta y)$ . The hologram of the zeroth-order component of the Fourier-spectrum  $T$  [ $H(\Delta x, \Delta y) = H(0, 0)$ ], will determine the background in the reconstructed image  $I$ , while the holograms of higher-order components [ $H(\Delta x, \Delta y)$ ] will determine its resolution. It is evident that each of the basic holograms can be reconstructed by the beam whose parameters coincide with those of one of the recording beams. The existence of reconstructed beams whose wavelengths differ from the recording wavelength becomes clear from the following consideration. Each elemental hologram is recorded by point-source beams, therefore any of its small parts is described by the constant grating vector  $K$ . This means that for an arbitrary wavelength  $\lambda$  in every point  $(x, y)$  of the elemental hologram, two rays (incident and diffracted) oriented at the Bragg angle to the grating vector  $K$  are determined unambiguously. Let us neglect the change in the grating vector  $K$  along the propagation path for each reconstructed ray in the hologram. In this case the lattice of rays combines to form only two beams which can be diffracted by this hologram and which, generally speaking, for an arbitrary wavelength  $\lambda$  are not spherical. Let us consider the hologram reconstruction by a spherical wave with coordinate  $(x_3, y_3)$  and determine the Bragg mismatch angle,  $\delta$ , for its rays at every point of their crossing the hologram. The assumption we have made above permits us to consider the diffraction of each pair of interacting rays independently and to calculate pointwise the diffraction efficiency of incident rays as a function of angle  $\delta$  in accordance with coupled-wave theory [6]. Thus we can calculate the intensity distribution in the reconstructed beam for every elemental hologram  $H(\Delta x, \Delta y)$ . Their sum corresponds to the Fourier-spectrum of the transparency  $t$  by which we can estimate the resolution in the reconstructed image.

As indicated in Fig. 3, rays from the recording  $(x_1, y_1)$ ,  $(x_2, y_2)$  and reconstructing  $(x_3, y_3)$  sources to an arbitrary point  $(x, 0)$  on the recording medium make an angle  $\theta_i$  where

$$\theta_i = \arctan\left(\frac{x_i - x}{y_i}\right), \quad i = 1, 2, 3. \quad (3.1)$$

The Bragg angle at the same point is

$$\theta_{Bragg} = \arcsin\left\{\frac{\lambda_1}{\lambda_2} \times \sin\left[\frac{\theta_1(x) - \theta_2(x)}{2}\right]\right\} + \frac{\theta_1(x) + \theta_2(x)}{2}, \quad (3.2)$$

which directly follows from the Bragg law written in common form [Ref. 5] for read-out  $\lambda_2$  and recording  $\lambda_1$  wavelengths. Consequently the Bragg mismatch angle  $\delta_{Bragg}$  is:

$$\delta_{Bragg}(x) = \theta_{Bragg}(x) - \theta_3(x). \quad (3.3)$$

We choose the coordinates of the point source reconstruction beam  $(x_3, y_3)$  in such a way that two of its rays, crossing the hologram at points  $(0, 0)$  and  $(c, 0)$ , make Bragg angles with the input plane (Eq. 3.2). We then



determine the mismatch angle  $\delta_{\text{Bragg}}$  for the rest of the rays of the reconstructed beam and insert into the relationship which expresses the angular sensitivity of a thick hologram [Ref. 6],

$$\eta = \exp\left[-\frac{2\alpha d}{c_s}\right] \times \exp[2i\xi] \times \frac{\left\{\exp\left[i(\xi^2 + v^2)^{0.5}\right] - \exp\left[-i(\xi^2 + v^2)^{0.5}\right]\right\}^2}{4 \times \frac{\xi^2 + v^2}{v^2}}, \quad (3.4)$$

$$\xi = \frac{2\pi n}{\lambda_2} \delta_{\text{Bragg}} d \sin\left(\frac{\theta_1 - \theta_2}{2}\right); \quad v = \frac{\chi d}{c_s}; \quad c_s = \cos\left(\frac{\theta_1 - \theta_2}{2}\right),$$

where  $d$  is the thickness of the hologram,  $\chi$  is a coupling constant.

This expression describes, in the exit plane of the hologram, the profile of the intensity of the diffracted wave which attains its maximum at points  $x=0$  and  $x=c$ . Notice that we are interested in the relative diffraction efficiency of diffracted rays versus only  $\delta_{\text{Bragg}}$  for each of them, so we can simplify Eq. (3.4) to

$$\frac{\eta}{\eta_0} = v^2 \sin^2 \left\{ \pi^{-1} \left[ v^2 + k \delta_{\text{Bragg}}^2(x) \right]^{0.5} \right\} \quad (3.5)$$

Here we took into account that the presence of loss has very little influence on the angular sensitivity [Ref. 6] and used Eq. (3.4) written for lossless gratings with real  $\chi$ . The constant  $v$  was measured experimentally. Figure 4 represents the relative intensity distribution profile (equivalent to normalized diffraction efficiency) of diffracted beams in the exit plane of the hologram, calculated for the elemental hologram  $H(0,0)$  [corresponding to the zeroth-order component of the Fourier-spectra  $T$  of transparency  $t$ ] for reconstructed beams with different values of the parameter ' $c$ '. Values of  $\lambda_1 = 0.45\mu\text{m}$  and  $\lambda_2 = 0.63\mu\text{m}$  were used for this and subsequent plots. The X-axis is in the hologram recording plane and the different values of ' $c$ ' are obtained by changing the location of the reconstruction point source,  $(x_3, y_3)$ . Optimized readout parameters will correspond to the portion of the hologram where the curves of Fig. 4 have enough diffraction efficiency, say not less than  $1/e$ , and are as flat as possible. In our experiments the hologram was about 3mm in extent, so  $c = 2\text{mm}$  would be optimal from Fig. 4.

Profiles of diffracted beams with optimized parameter ' $c$ ' calculated for several recording set-ups of  $H(0,0)$  holograms (with different orientations and average spatial frequencies of recording beams) are shown in Fig. 5. The diffraction of the beam, optimized for the reconstruction of the hologram  $H(0,0)$ , from the holograms  $H(\Delta x, \Delta y)$ , corresponding to the higher-order components of the Fourier-spectrum  $T$ , is shown in Fig. 6. These plots represent the sum intensity distribution of beams diffracted by holograms  $H(\Delta x, \Delta y)$  and  $H(-\Delta x, -\Delta y)$ , where we use the fact that symmetric components of the Fourier-spectrum contain the same information. From Fig. 6, we see that the relative diffraction efficiency decreases with increasing values of  $r$ , corresponding to holograms of higher components of the Fourier-spectrum,  $T$ . Thus the reconstruction system is acting like a low-pass filter, and one can use this curve to define an effective spatial cutoff frequency, at some particular value of relative diffraction efficiency ( $1/e$ ).

Let's consider now in more detail how the intensity profiles of beams, diffracted by elemental holograms (Fig. 4 to 6) can be utilized to determine the resolution and intensity distribution in the reconstructed image,  $t$ . Every point  $P$  of the recording transparency,  $t$  is formed by a cone of rays connecting it with points of the Fourier-spectrum (Fig. 4), each of which we took as an elementary point-source object beam of the elemental hologram. The part of the transparency,  $t$ , in the vicinity of point  $P$  will be reconstructed with resolution  $h$ , if all rays of a cone with base radius

$$r = \frac{0.61\lambda_1 D}{h} \quad (3.6)$$

have enough diffraction efficiency ( $\eta > \frac{\eta_0}{e}$ ), where  $r = (\Delta x^2 + \Delta y^2)^{0.5}$  - is one of the coordinates of the

Fourier-plane of the transparency  $t$  and  $D$  is the distance between the plane of transparency  $t$  and its Fourier-transform plane,  $T$ . Taking into account the behavior of the plots in Fig. 6, the proper diffraction efficiency of only edge cone rays corresponding to the maximal-order components of the Fourier-spectrum will provide the required resolution. Then, it is easy to see that the intensity distribution of the reconstructed

beam at the image plane corresponds to a profile of the beam diffracted by the  $H(0,0)$  hologram at its exit plane, reduced in size by  $D_2 \cos \theta_{\text{aver}} / D_1$ , where  $D_1$  and  $D_2$  are the distances between the Fourier-plane of image  $i$  and, respectively, the hologram and the plane of the image;  $\theta_{\text{aver}}$  is the average incident angle of the reconstructing beam. Thus, the intensity and resolution in an arbitrary part of the reconstructed image  $T$  can be estimated by the profile of two beams diffracted by elemental holograms  $H(0,0)$  and  $H(\Delta x, \Delta y)$ , where  $\Delta x$  and  $\Delta y$  obey the condition of Eq.(3.6).

#### 4. Multichannel correlation schemes.

The main results of the previous two sections which can be used to advantage in building multichannel correlators are:

1. The ability to simultaneously record several holograms in thick BR films that can be reconstructed selectively.
2. The capability of reconstructing volume holograms using different wavelengths. The resolution of a reconstructed image can be sufficiently high (comparable with TV standards). The simplified method provided for computing the resolution and the DE of the reconstructed beam allows one to assess the information loss in each particular instance of recording.

Using the above results, let's consider one of the possible correlator setups that has several independent channels for processing the input signal (Fig. 7). Each of the channels is acting in a regime analogous to that of a CFP. Changes that have been introduced into the setup (for the reasons which will come clear below) include:

- In the correlator of Fig. 7 the exact Fourier-transform is changed to the scaled Fourier-transform.
- Instead of a reference beam with a plane wavefront, we use a highly convergent one.

Holograms  $H_i$  have been recorded using optical signals  $S_{1i}$  (filter signal) formed by the input setup  $SLM_1$  and one of the optical fibers  $OF_i$  and have been used as a matched filter for the signal  $S_{2i}$  (master signal) input into the system by  $SLM_2$ . Hologram multiplexing is done using the method described in Section 2. For the setup to be used as a multichannel correlator the following element adjustments should be made:

The red beam 2 illuminating  $SLM_2$  is formed by the lens  $L_2$  and  $N$  pieces of fiber  $OF_2$  and represents  $N$  converging spherical waves  $u_i$ . Parameters of each of the spherical waves are adjusted so that the diffraction requirements of one of the holograms,  $H_i$ , recorded without modulation (by  $SLM_{1,2}$ ) are met. In this case each of the spherical beams  $H_i$  will reconstruct one of the virtual images,  $Im_i$  of beam  $R_i$ . The method applied to form a Fourier-transform allows one to change the transform's scale by shifting  $SLM_2$  longitudinally along the axis of the lens  $L_2$ , thus compensating for scale changes caused by different wavelengths of the signals  $S_1$  and  $S_2$ . The  $SLM_2$  position with respect to the axis  $L_2$ , which corresponds to an equal scale of the optical signals  $S_1$  and  $S_2$ , is the same for all holograms. In the direction normal to the optical axes of the lenses ( $X_{1,2}$ ) the image displayed on  $SLM_2$  is shifted with respect to the image of  $SLM_1$ , depending on which channel the image of  $SLM_1$  has been recorded. To compensate for this shift along the  $X$ -axis of  $SLM_2$ , adequate shifts are introduced along the  $X$ -axis of  $SLM_1$  during the recording of the hologram-filters  $H_i$ . Thus the correlator of Fig. 7 functions as follows:  $N$  blue input optical signals  $S_{1i}$  are applied with the frequency  $\nu$  to the input of  $SLM_1$ , forming  $N$  hologram-filters  $H_i$  on the BR (details in Sec. 2). Combined red beam 1 illuminating  $SLM_2$  provides diffraction on any of  $N$  channels (virtual image of one of the  $R_i$ ) whenever the image of  $SLM_2$  correlates with one of the images on  $SLM_1$ . It is worth noting that the Bragg diffraction regime of hologram-filters  $H_i$  provides a possibility of using independent channels, but limits the display accuracy of the optical signals. For example, for recording beams having a spatial frequency of  $(1/\lambda_{\text{blue}})$ , a BR thickness of  $100\mu\text{m}$ , and  $D_1$  and  $D_2$  (distance between the BR and  $SLM_1$ , and  $SLM_2$ , respectively) of 10 cm, the images have to be displayed with at least 0.5mm accuracy. In such a configuration the correlator can be only used to search for identical images. In this case one of the most attractive advantages of a CFP is lost, namely, the possibility of finding an image using an image fragment. However such a restriction can be substantially relaxed by decreasing the spatial frequencies of the beams which record hologram-filter  $H_i$ . Consequently, the number of channels is decreased.

The above described correlation scheme in which signals have different wavelengths has the following disadvantages:

1. Resolution is limited (Sec. 3) which in turn limits the amount of information being processed.

2. Differences in the geometry of the optical signals  $S_1$  and  $S_2$  caused by different wavelengths make the system very alignment sensitive.

The next scheme, in which the signals  $S_{1i}$  and  $S_2$  as well as the correlation signal  $R_i$  have the same wavelength ( $\lambda_1 = 0.45\mu$ ), is free from the above disadvantages (Fig. 8). In addition, the setup allows one to use only one SLM. As in Fig. 7, the processed optical signals consist of filter signals  $S_{1i}$  that were recorded on BR as hologram-filters, and master signal  $S_2$  that should be matched with the hologram-filters. Signals  $S_{1i}$  and  $S_2$  are alternately displayed on the SLM with the frequency  $2\nu$  (each signal is displayed with frequency  $\nu$ ).  $N$  reference beams  $R_i$  are switched with frequency  $\nu$  and synchronized with the signals  $S_i$  using a method analogous to one used in Section 2. The separator  $K$  is implemented with two rotating shutters, and  $Sc_{1,2}$  is used to separate correlation signals in the output plane (Fig. 8). Red light illuminating the BR is used for transferring the BR into the M-state in preparation for recording by blue light. In Fig. 9, synchronization of all elements composing the correlator is shown. It can be seen from the figure that the pair  $(R_i, S_i)$  which

records the hologram  $H_i$  exposes the BR in the time interval  $\left(\frac{2n-1}{\nu}, \frac{2n}{\nu}\right)$ . During the intervals

$\left(\frac{2n}{\nu}, \frac{2n+1}{\nu}\right)$  the recording medium is illuminating only by signal  $S_2$ . In the output plane the separator  $K$

in each moment of time is closed for beams  $R_i$  and in the interval  $\left(\frac{2n}{\nu}, \frac{2n+1}{\nu}\right)$  it is open for the first

diffraction orders of the signals  $S_2$  on the hologram  $H_i$ , which represents the correlation signal between  $S_{1i}$  and  $S_2$  multiplied by a constant factor.

## 5. Conclusion

The capability of a BR-based thick hologram for pattern recognition systems was considered. Real-time recording of several holograms and their selective reconstruction was demonstrated. We showed that using volume holograms in the Van-der-Lugt correlator with frequency plane allows one to perform multichannel processing of optical signals. Correlators in which the compared signals have both different and the same wavelength are proposed. It was shown that these setups allow one to increase data throughput significantly. We also suggested a simplified calculation method for estimating the loss of information due to recording and restoration by differing wavelengths.

## Acknowledgments

We thank Bend Research, Inc. for preparation of the BR-films. This work was supported by the NASA Ames Research Center, whose support is sincerely appreciated.

## References

1. N. Hampp, R. Thoma, C. Brauchle, and D. Oesterhelt, Appl. Opt. **31**, 1834 (1992).
2. R. Thoma, M. Dratz, and N. Hampp, Optical Engineering **34**, No. 5 (1995).
3. R. Thoma and N. Hampp, Optics Letters **17**, No. 16 (1992).
4. G. Barbastathis, M. Levene, and D. Psaltis, Applied Optics **35**, 2403 (1996).
5. R.J. Collier, C. B. Burckhardt, and L. H. Lin in: *Optical Holography*, 128, (Acad. Press, New York, London, 1971).
6. H. Kogelnik, "Coupled wave theory for thick hologram gratings", Bell. Syst. Tech. J. **48**, 2909 (1969).

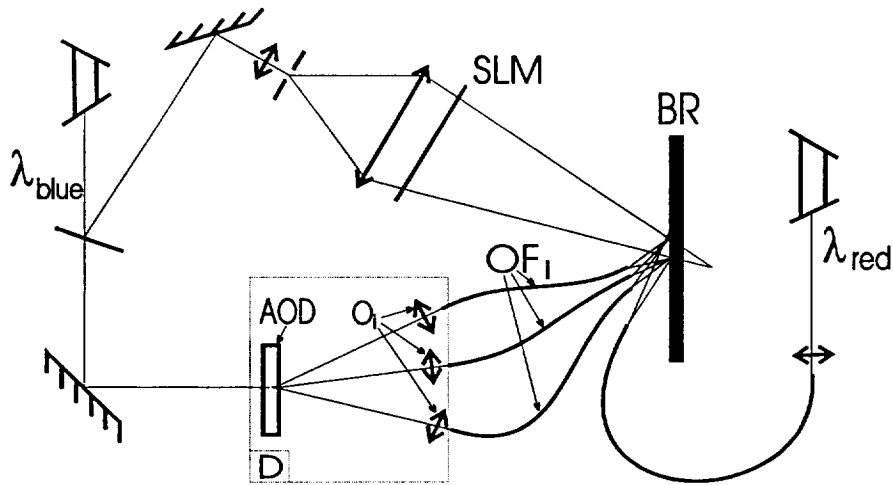


**Fig. 1** Hologram multiplexing setup: SLM is spatial light modulator; OF<sub>i</sub> are optical fibers forming reference beams Ri: node D consist of an acousto-optic deflector(AOD) and micro objectives O<sub>i</sub>; BR is Bacteriorhodopsin recording medium

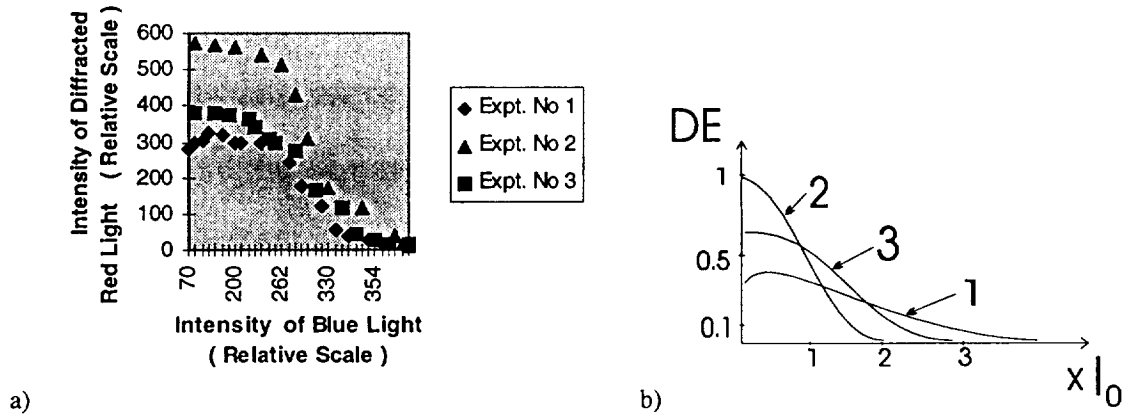


**Fig. 2:** a) is relative intensity of output signal versus intensity of input signal for various values of ratio  $I_{red}/I_{blue}$  ( $I_{red}/I_{blue}=5, 1, 2$  for Curves 1, 2, 3, respectively), b) are the same curves given in units of  $I_0$ (average intensity of the recording blue beams).

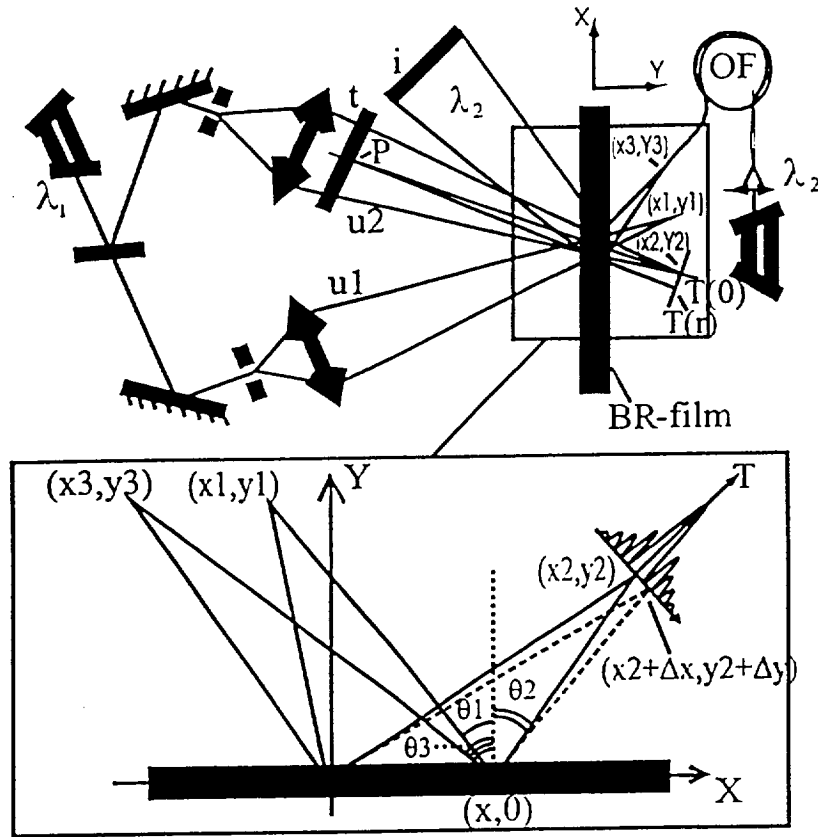


Fig. 3: Geometry of recording and read-out rays. Here  $t$  and  $T$  denote the transparency and its Fourier-transform respectively;  $i$  - reconstructed image; OF - optical fiber

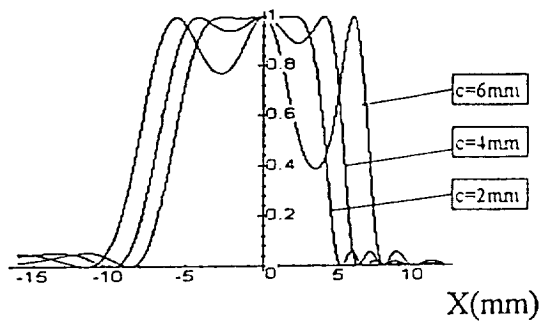


Fig. 4 Normalized diffraction efficiency of  $H(0,0)$  versus hologram plane position for various 'c' parameters

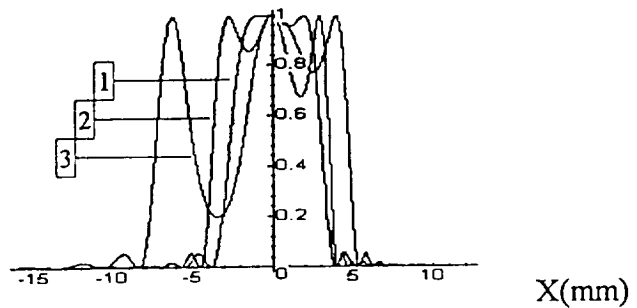
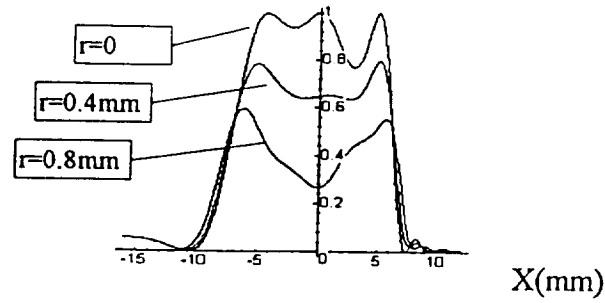
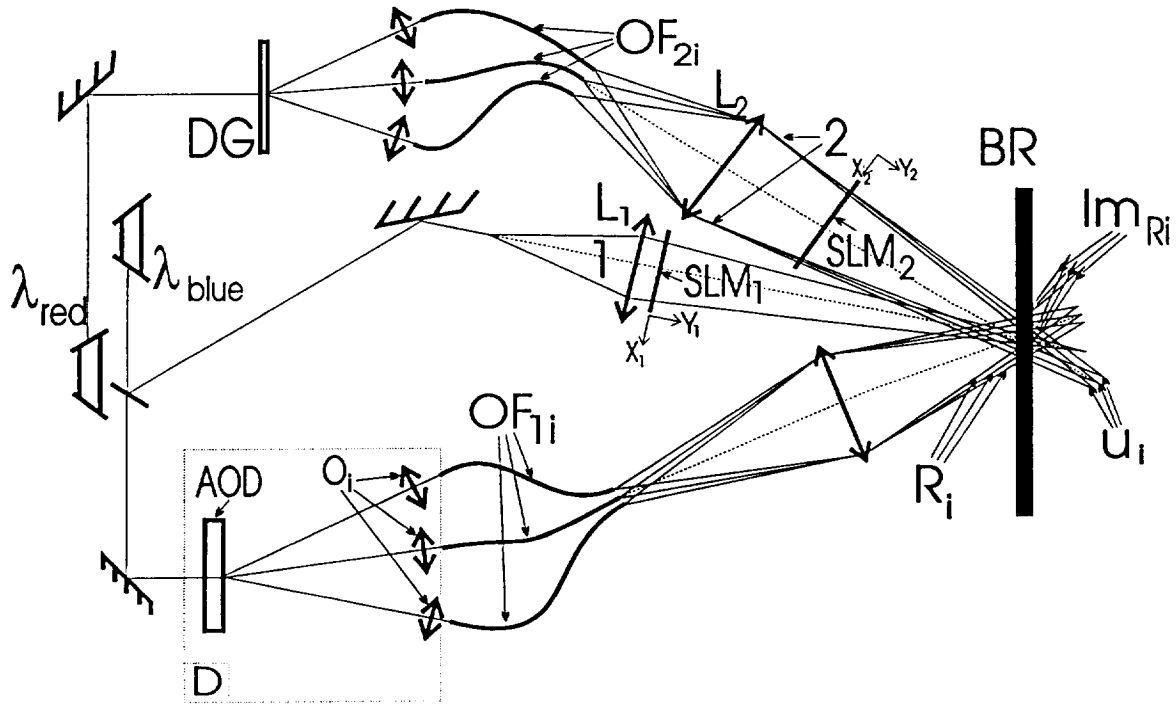


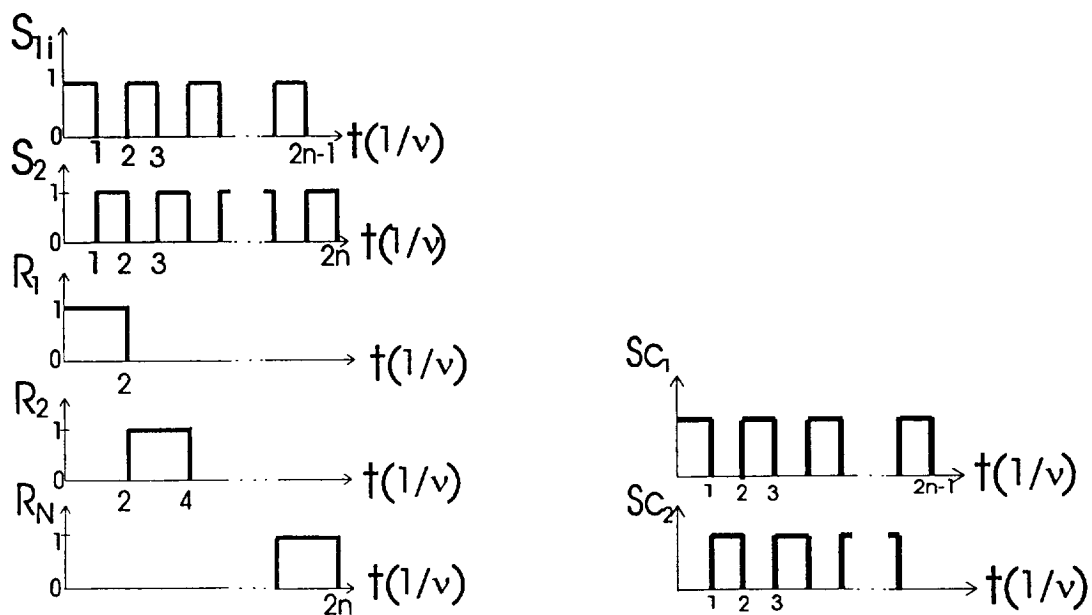
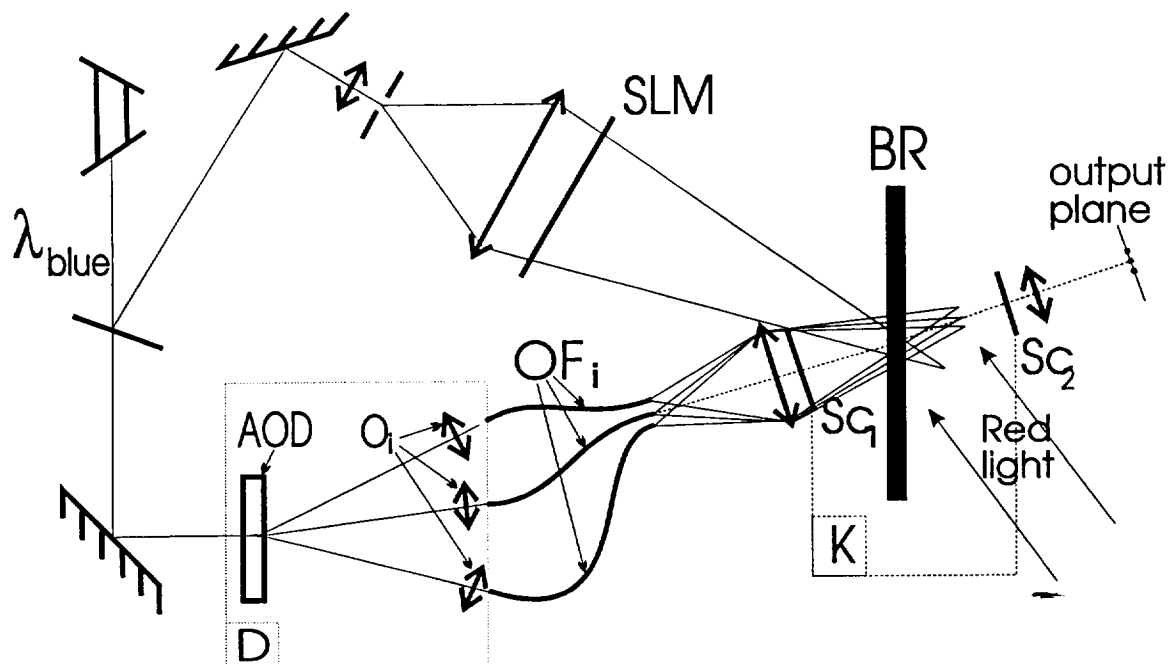
Fig. 5: Normalized diffraction efficiency for Fig. cases:  $(x_1, y_1) = (7, 10)$ ,  $(x_2, y_2) = (6.5, 10)$ ,  $(8, 10)$ ,  $(5, 10)$  - plots 1, 2, and 3, respectively.



**Fig. 6:** Normalized diffraction efficiency of elemental holograms with various  $r$  versus hologram plane position



**Fig. 7** Multichannel correlation setup processing signals with different wavelengths:  $SLM_{1,2}$  are spatial light modulators;  $L_{1,2}$  are lenses performing post-lens Fourier-transforms; 1 is a blue beam forming the object beam  $S_{1i}$  for hologram  $H_i$  recording;  $R_i$  are reference beams for recording the hologram  $H_i$ ; 2 is a red beam ( $N$  spherical convergent beams  $u_i$ ) which, illuminates  $SLM_2$ , to form the master signal  $S_2$ ; node D (acousto-optical modulator and  $N$  microobjectives) couples the blue laser beam with each of the  $OF_{1i}$ ;  $Im_{Ri}$  is one of the virtual images of the reference beam  $R_i$  reconstructed in red light; and DG is a diffraction grating using as a beam splitter.



# **GRATING-TYPE SPATIAL LIGHT MODULATOR IN BACTERIORHODOPSIN FILM\***

**Arkady S. Bablumian, Thomas F. Krile, David J. Mehrl,**

**John F. Walkup**

**Optical Systems Laboratory**

**Department of Electrical Engineering**

**Texas Tech University**

**Lubbock, Texas 79409**

**\* Research Supported By NASA Ames Research Center**



# **Introduction**

The process of real-time recording and reconstruction of holographic gratings in Bacteriorhodopsin(BR) films is used for constructing an optically-addressable spatial light modulator (SLM).

The purpose of our work was to explore such an architecture for overcoming the following drawbacks inherent in the traditional BR-based SLM:

- low contrast
- fixed SLM characteristic response curve
- limited spectral range

## **The basic principles of signal transformation in a grating-type SLM**

Upon red light exposure, BR molecules photochromically undergo the full photocycle through several intermediate states. Some of the states are photoreversible and can be driven directly to the initial BR-state by exposure to blue light. Upon simultaneously exposing the BR film to red and blue light, the equilibrium between the numbers of molecules in both states is established depending on the ratio of relative beam intensities. This mechanism explains the process of real-time recording and reconstruction of the holographic grating (without erasing).

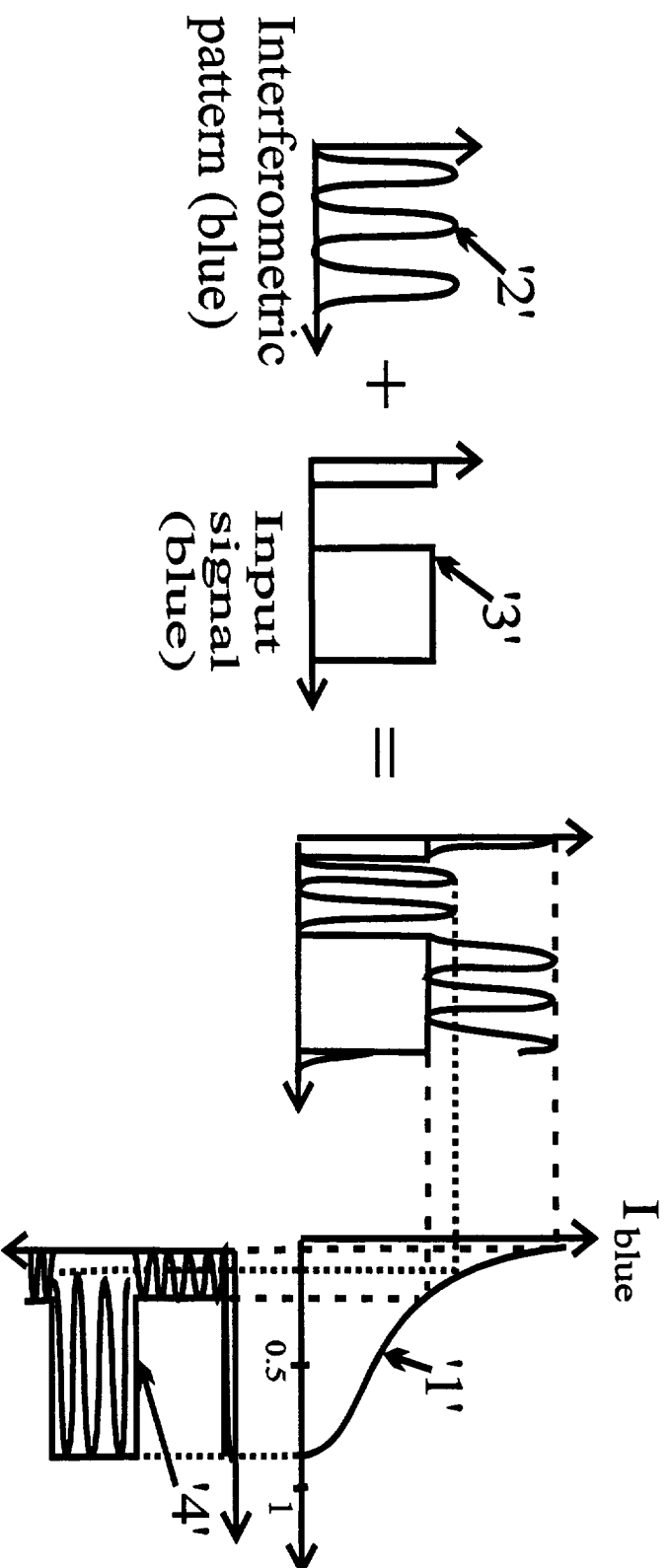


**Fig. 1** (caption below)

Curve '1' represents the percentage of excited BR molecules relative to those in the initial state versus the intensity of the blue light exposing the BR film (with simultaneous constant red light exposure).

Curves '2' and '3' represent the interferometric intensity pattern of the blue beams illuminating the BR film and the input blue signal, respectively(see Fig. 2). The resulting spatial modulation of the absorption/refractive index parameters of the BR film is described by Curve 4. The red beam performs a dual function: (1) excites the BR molecules and (2) reads out the holographic grating.

Curve '1' in Fig. 1 permits us to qualitatively explain the possibility of varying the diffraction efficiency of the recording grating(output signal '4') by modulating the intensity of the input blue signal '4'. The blue input signal shifts the interferometric pattern into the nonlinear range of the characteristic curve '1', thus changing the diffraction efficiency of the recording grating.

# **BINARY, OPTICAL SIGNALS**

## Experimental setup for transformation of blue signal (incoherent or coherent) into the coherent red signal

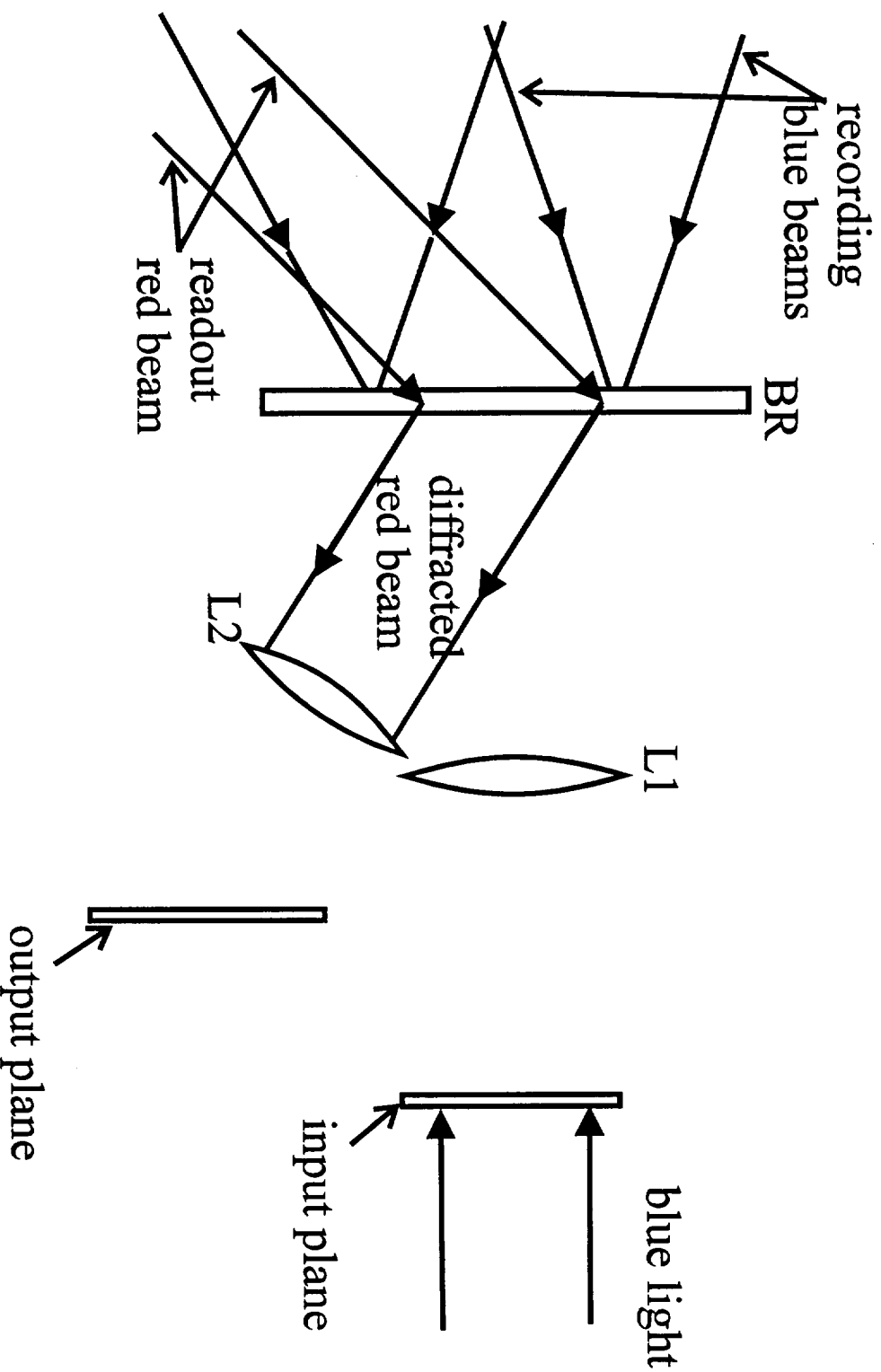
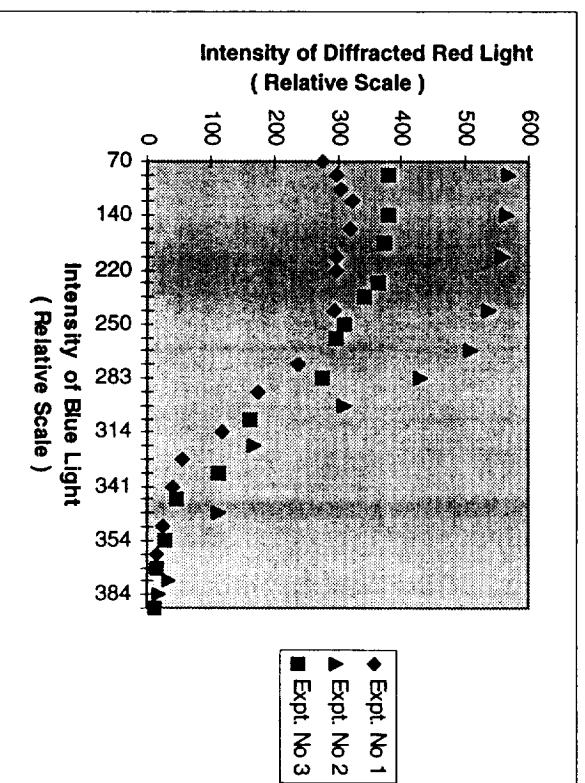


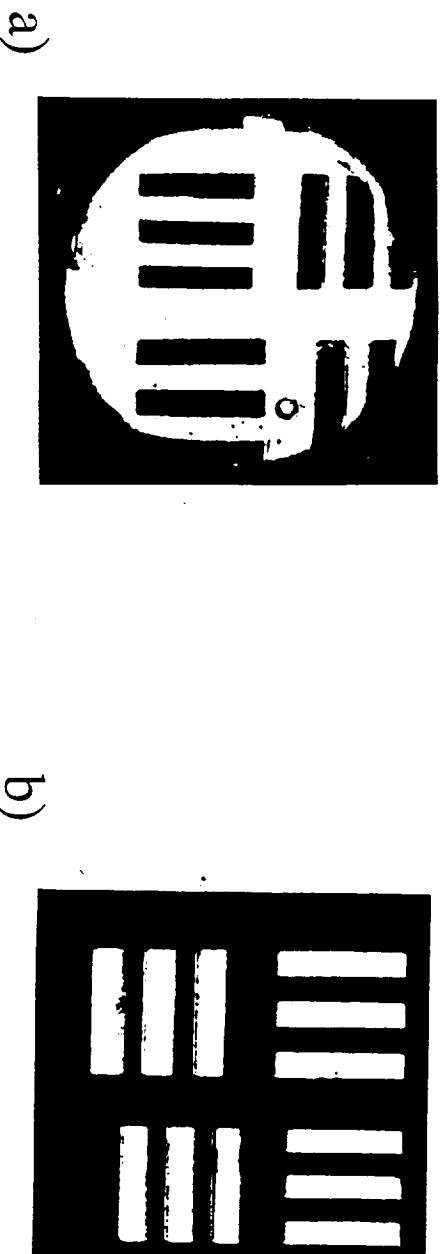
**Fig.2:**  $L_1$  and  $L_2$  are lenses, which, respectively, project (1) the input plane on the BR film surface and (2) the plane of the BR film onto the output plane

**Fig. 3:** Relative intensity of output signal versus intensity of input signal (input signal can be either coherent or incoherent) for various values of  $I_1/I_2$  ( $I_1/I_2=5, 1, 2$  for Curves 1, 2, 3, respectively), where  $I_1$  and  $I_2$  are the intensities of the recording blue beams and the readout red beam (Fig. 2).



As one can see from these plots, the SLM transformation regime can be changed by changing  $I_1/I_2$ .

**Fig.4:** Photos of the output plane image corresponding to the input transparency, T, for two cases: (a) with the system shown in Fig. 2; and (b) with the BR film replaced by a mirror.



Comparison of the resolution and contrast in these photos permits one to conclude that there is no loss of information between the input and output signals. In our experiments these parameters were limited by the projection features of objective lenses L1 and L2 (Fig.2) and were found to be 100 lines-pairs/mm for the resolution and 120 for the contrast.



# GRAY-SCALE OPTICAL SIGNALS



## Mechanism of signal transformation in the SLM setup of Fig. 5

Light propagation in BR is fundamentally a nonlinear process associated with the changing of parameters in the recording medium (absorption and refractive index). The blue beams used in recording the grating (Fig.5) at the same time experience a self-diffraction process. The diffraction efficiency of the grating can be changed by the red light which changes the relative quantities of excited BR molecules(see Fig.1). In this setup we use one of the diffracted blue beams (beam 3) as an output signal and the red beam 4 as the input signal (Fig. 5). The characteristic response curve expressing the dependence of output signal intensity as a function of input signal intensity is shown in Fig. 6

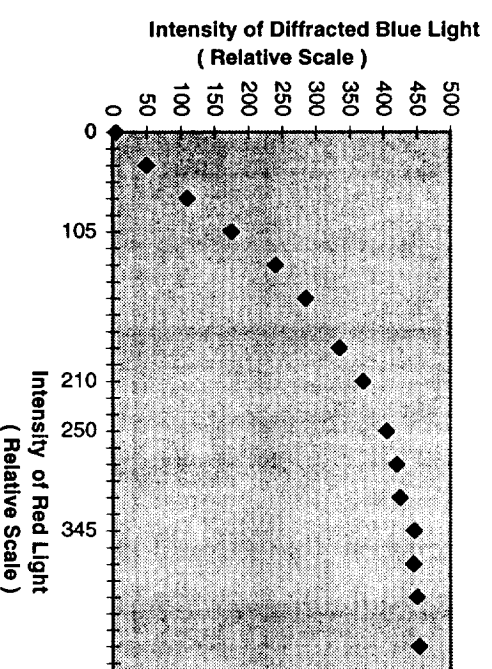


**Fig. 6:**

Comparing this curve(Fig. 6) with the curves of Fig. 3 one can see the following differences between the SLM setups of Fig. 2 and Fig. 5:

- The SLM setup of Fig.2 can be used for binary signals having a relatively high intensity; the modulation process inverts(contrast reversal) the input signal.
- In contrast with this setup, the SLM setup depicted in Fig.5 provides high sensitivity. It can be used for transformation of gray-scale signals having a wide dynamic range, providing a direct transformation process(positive input signal into positive output signal). The main obstacle for utilizing this setup consists of difficulties in separating the zero and first order components of the diffraction pattern which propagate over the same path (the 0-th order of beam '1' coincides with the 1-st order of beam '2', Fig. 5). To separate them we used the revolving screens  $S_1$  and  $S_2$  which have time-dependent transmittance functions,  $T_1(t)$  and  $T_2(t)$ , that are opposite in phase. When applied together, these screens are opaque for the zero order of the diffraction pattern (beam '1'), but are transparent for its first order (beam '3').

# Conclusions

The grating-type SLM is characterized by the following features:

- high contrast
- high sensitivity
- a flexible transformation regime for optical signals which can be varied by changing the SLM parameters(relative intensities of the beams forming the active area of the SLM) to provide:
  - either a linear regime(for transformation of both binary and gray-scale optical signals);
  - or a nonlinear regime(for a broad range of real-time data processing applications);
- the SLM, with this geometry, can work in both incoherent-to-coherent and coherent-to-coherent optical transformation regimes, with and without changing the input signal's wavelength
- it can also work in an infra-red readout mode.